Adaptive time stepping for explicit euler implementation of spherical and non-spherical particle speed up

Gernot Boiger[1], Marianne Mataln[1] and Wilhelm Brandstätter[2]
[1]ICE Strömungsforschung GmbH, Hauptplatz 13, 8700 Leoben, Austria
[2]Montanuniversität Leoben, Franz-Josefstrasse 18, 8700 Leoben, Austria
www.ice-sf.at

ABSTRACT

Numerical implementation schemes of drag force effects on Lagrangian particles can lead to instabilities or inefficiencies if static particle time stepping is used. Despite well known disadvantages, the programming structure of the underlying, C++ based, Lagrangian particle solver led to the choice of an explicit EULER, temporal discretization scheme. To optimize the functionality of the EULER scheme, this paper proposes a method of adaptive time stepping, which adjusts the particle sub time step to the need of the individual particle. A user definable adjustment between numerical stability and calculation efficiency is sought and a simple time stepping rule is presented. Furthermore a method to quantify numerical instability is devised and the importance of the characteristic particle relaxation time as numerical parameter is underlined. All derivations are being conducted for (non-)spherical particles and finally for a generalized drag force implementation. Important differences in spherical and non-spherical particle behaviour are pointed out.

1. INTRODUCTION

A Lagrangian particle solver, based on the Open Source Computational Fluid Dynamics (CFD) software OpenFOAM® [18, 19] was developed as described in (Boiger & Mataln, 2008, [1, 2] & [20, 21]). The simulation is supposed to model particle deposition effects in deformable filter fibre media at low Reynolds and Knudsen numbers.

Within the course of programming, all particle modelling was based on the calculation of individual, explicitly formulated force effects, [2, 20]. Because of the wide variety of individual forces, and the specific set up of the code, the application of commonly used discretization schemes such as the Runga Kutta Scheme [10], or semi analytical approaches as described in (Göz, Lain & Sommerfeld, 2006, [11]), was found to be disadvantageous. Therefore an explicit EULER implementation of force effects on particle movement was selected. At constant time step Δt the EULER scheme constitutes an approximation of the semi analytical approach of order $O(\Delta t)$, [10]. A well known problem of the simple, explicit EULER implementation is the occurrence of numerical instabilities. It has to be addressed.

So far the OpenFOAM® based, Lagrangian particle solvers have used a constant number of user defined Subcycles J, to account for particle time scales that are smaller than fluid time scales. The simple relationship between fluid time step Δt_f, particle time step Δt_p and the number of particle Subcycles J reads:

$$J = \left\lceil \frac{\Delta t_f}{\Delta t_p} \right\rceil = const \tag{1}$$

with $J \in Z$, $\Delta t_p \leq \Delta t_f$, $J \geq 1$ and J = const. The ceiling function $\lceil \ \rceil$ is of course preferred here to a floor function $\lfloor \ \rfloor$, in order to be on the safe side. Per definition particle time steps can not become greater than fluid time steps. Once the number of Subcycles is selected, it remains statically linked to the fluid time step, regardless of particle dimensions, material properties, or flow conditions. As a consequence, static time stepping can lead to inefficiencies and numerical instabilities.

This paper proposes a simple method of adaptive particle time stepping, taking into account the properties of each individual particle, such as particle mass m_p, particle density ρ_p and properties of the local fluid region, such as dynamic fluid viscosity μ_f as well as fluid velocity u_f, and particle velocity u_p so that:

$$J(\mu_f, u_f, u_p, \rho_p, \Delta t_f, m_p) = \left\lceil \frac{\Delta t_f}{\Delta t_p(\mu_f, u_f, u_p, \rho_p, m_p)} \right\rceil \tag{2}$$

Furthermore this work presents a way to quantify the degree of numerical particle stability, that goes along with each chosen particle sub time step. Based on these results an adaptive time stepping method is worked out, that allows the user to select accuracy and efficiency of the explicit EULER force effect modelling.

2. EXPLICIT EULER TEMPORAL DISCRETIZATION OF DRAG FORCE EFFECT ON (NON-) SPHERICAL PARTICLES

The simple, explicit Euler, temporal discretization of particle movement under the influence of external forces for th jth time step can be written as:

$$\bar{u}_p\left(t_j = t_{j-1} + \Delta t_{p,j}\right) = \bar{u}_p\left(t_{j-1}\right) + \frac{1}{m_p} \cdot \sum_{i=0}^{N} \bar{F}_{i,j} \cdot \Delta t_{p,j} \tag{3a}$$

Issues concerning numerical instability, stemming from the explicit EULER, temporal discretization, are at the focus of this paper. Those instabilities are limited to particle–fluid interaction force effects and do not concern momentary forces caused by events such as particle–particle, particle-wall or particle-fibre impacts (Boiger, Mataln, 2008, [2, 21]). Therefore particle-fluid forces have to be inspected in detail.

2.1. PARTICLE–FLUID INTERACTION: DRAG FORCES

The *Basset Bousinesque Oseen* (BBO) equation offers a complete, mathematical quantification of all possible interaction forces acting on any object being immersed in a fluid, [5, 11]. Going on from this generalized description, the problem needs to be simplified. Therefore the simple case of a particle, slowly speeding up in a uniform flow field shall be considered. The governing particle momentum equation (PME) is then mainly governed by fluid drag- and lift forces, F_d and F_h respectively, so that:

$$m_p \frac{d\bar{u}_p}{dt} = \bar{F}_d + \bar{F}_h \tag{3b}$$

Lift forces are only relevant for arbitrarily positioned, non-spherical particles and shall be disregarded here.

The general, well known formulation of the fluid drag force, for 1D, uniform flow conditions reads:

$$F_d = \frac{1}{2} c_d(\mathrm{Re}_p) \rho_f A_f \cdot u_{rel}^2 \tag{4}$$

Here c_d is the drag coefficient, A_f is the projected frontal surface area, u_{rel} is the relative fluid–particle velocity, ρ_f is the fluid density and Re_p is the particle Reynolds number, which is defined as:

$$\mathrm{Re}_p = \frac{u_{rel} D_{sph}}{\eta_f} \tag{5}$$

In Equ.5 η_f is the kinematic fluid viscosity and D_{sph} is the particle diameter of a volume equivalent sphere. D_{sph} is defined as:

$$D_{sph} = \sqrt[3]{\frac{6m_p}{\pi \rho_p}} \tag{6}$$

Here m_p is the particle mass.

For spherical particles and low Reynolds numbers, Stokes' law is applicable to calculate the drag coefficient:

$$c_d = \frac{24}{\mathrm{Re}_p} \tag{7}$$

In total there are well over 30 equations (Haider, Levenspiel, 1988, [12]) in literature, relating the drag coefficient of spherical particles to the Reynolds number.

The amount of equations in literature, describing the drag coefficient of non–spherical, e.g. ellipsoid, particles is significantly lower. Reviews on this subject have been conducted e.g. by (Haider, Levenspiel, 1988, [12]) and (Hölzer, Sommerfeld, 2007, [13]).

Hölzer & Sommerfeld have furthermore presented a c_d correlation formula for ellipsoids, that is reportedly valid over the entire range of Reynolds numbers [13]. The authors have compared their formula, shown in Equ.8, to a wide range of experimental results for spheres, isometric particles, cuboids, cylinders, disks and plates and report mean, relative deviations of 14.1%. This number compares to values of significantly more than 100% for several other non-spherical drag force formulations in use. Consequentially this work will adopt it for the

discussion of non–spherical drag force implementation and the related time stepping problems.

$$c_d = \frac{3}{\mathrm{Re}_p}\frac{1}{\sqrt{\Phi_{length}}} + \frac{16}{\mathrm{Re}_p}\frac{1}{\sqrt{\Phi}} + \frac{3}{\mathrm{Re}_p}\frac{1}{\Phi^{\frac{3}{4}}} + 0.4210^{0.4(-\log\Phi)^{0.2}}\frac{1}{\Phi_{\mathrm{cross}}} \tag{8}$$

In Equ.8, Φ denotes the sphericity of the particle, Φ_{cross} stands for the crosswise sphericity and Φ_{length} is the lengthwise sphericity.

2.2. PARTICLE SPEED UP

Previous works of e.g. Lain, Göz & Sommerfeld, [7]–[11], have considered the case of gravitational particle settling and specifically the value of the terminal particle settling velocity to study numerical instabilities. Since gravitational effects play a negligible role in the context of automotive oil filtration [1], a different method to numerically and analytically study time stepping- and instability effects was devised.

Hereby the case of a particle which speeds up in a uniform flow field shall be analyzed. The ratio between particle–wall distance and particle diameter shall be considered as large and any additional effects on the Lagrangian PME shall be disregarded as described above. Therefore, in extension of Equ.3, the simplified particle momentum equation reads:

$$\frac{du_p}{dt} = c_d \frac{\rho_f A_f}{\rho_p V_p} u_{rel}^2 \tag{9}$$

In this context u_p is the particle velocity, u_{rel} is the relative particle–fluid velocity, V_p is the particle volume, ρ_p is the particle density and ρ_f the fluid density.

2.2.1. Speed up of spherical particles

The characteristics of the speed up curve of any particle being inserted at particle velocity $u_p = 0$ m/s, into a fluid flow of uniform velocity u_f, depend mainly on the implementation of the drag coefficient. For spherical particles and low Reynolds numbers the analytical solution for the development of particle velocity from *zero*, infinitely close to u_f, against time, can be found easily [6]. It reads:

$$u_p = u_f - u_{rel,0} \cdot e^{-\frac{18\mu_f}{\rho_p D_{sph}^2}t} \tag{10}$$

Here $u_{rel,0}$ is the relative particle-fluid velocity at t = 0s. Figure 1 shows the plot of an exemplary, spherical particle speed up curve and the usual, graphical interpretation of the characteristic, spherical particle relaxation time $\tau_{p,sph}$ (see chapter 3.1).

2.2.2. Speed up of non–spherical particles

In the case of non–spherical particle speed up, an analytical solution for the speed up curve can not be found that easily. By inserting the c_d correlation of Equ.8 into the simplified PME of Equ.9 and by consequential integration over time and relative particle–fluid velocity, the following expression is reached:

$$t(u_{rel}) = \frac{C_0}{C_1}\left(\frac{2C_2\, ArcTan\left[\dfrac{C_2 + 2C_3\sqrt{u_{rel}}}{\sqrt{-C_2^2 + 4C_1C_3}}\right]}{\sqrt{-C_2^2 + 4C_1C_3}} + \log(u_{rel}) - \log(C_1 + C_2\sqrt{u_{rel}} + C_3 u_{rel}) \right)\Bigg|_{U_{rel,0}}^{U_{rel}} \tag{11}$$

Here the constants C_0, C_1, C_2 and C_3 are:

$$C_0 = \frac{2V_p\ \rho_p}{A_{f,ell}\rho_f} \tag{12}$$

Where V_p is the particle volume and $A_{f,ell}$ is the frontal area of an ellipsoid particle, projected onto a plane, perpendicular to the relative fluid-particle velocity vector.

$$C_1 = 8\frac{\mu_f}{D_{sph}}\frac{1}{\sqrt{\Phi_{length}}} + \frac{2}{\sqrt{\Phi}} \tag{13}$$

$$C_2 = 3\sqrt{\frac{\mu_f}{D_{sph}}}\frac{1}{\Phi^{\frac{3}{4}}} \tag{14}$$

$$C_3 = 0.421^{0.4210^{0.4(-\log\Phi)^{0.2}}\frac{1}{\Phi_{cross}}} \tag{15}$$

Equ.11 however, is transient in nature, therefore a solution for $u_p = f(t)$ can only be obtained numerically. The Newton Raphson procedure [4] is used to get a plot of the results of the explicit solution for u_p out of Equ.11 (see Figure1).

One focus of this paper is to point out the significant difference in speed up behaviour between spherical- and non-spherical particles, which share the same volume equivalent spherical diameter. Figure 1 shows a direct comparison of the speed up behaviour of an exemplary spherical particle and a non-spherical particle of equal mass and volume, with arbitrary sphericity and under matching flow conditions. Assuming the qualitative, physical correctness of the non-spherical drag implementation of Equ.8, the decreased sphericity, leads to decreased particle relaxation time, increased drag forces and thus to faster particle speed up.

2.3. NUMERICAL INSTABILITY OF EXPLICIT EULER DRAG FORCE EFFECT IMPLEMENTATION

For a given, exemplary fluid time step, fluid properties, spherical particle dimensions, particle density and flow conditions, a variation of particle Subcycles easily reveals the weakness of static particle time stepping. Figure 2 shows a plot of three numerically calculated, spherical

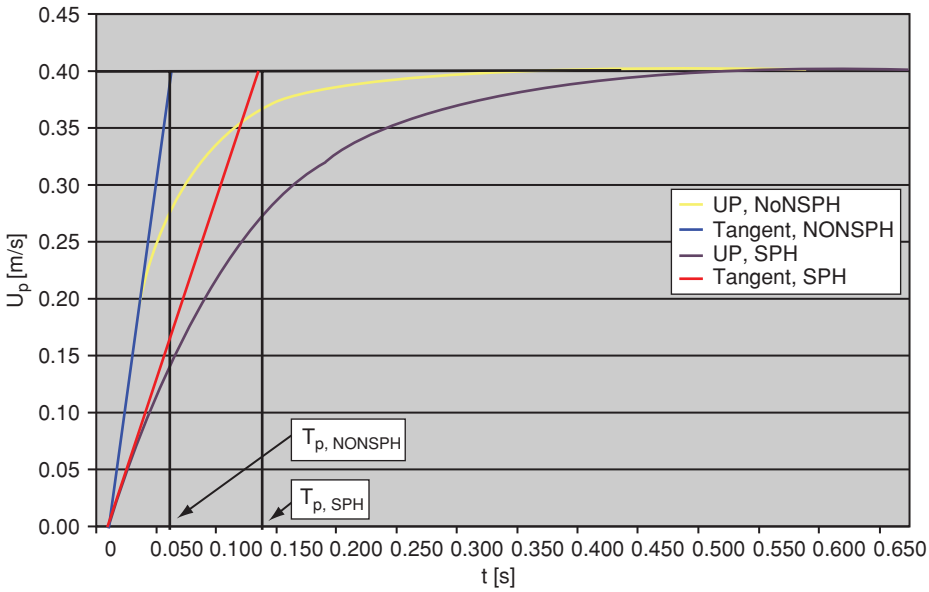

Figure 1 Plot of particle velocity u_p[m/s] against speed up time t[s]. Comparison of spherical- and non-spherical particles with the same mass and D_{sph} = 0.01m, speeding up under matching, uniform 1D flow conditions, μ_f = 0.1Pas, u_f = 0.4m/s. Graphical interpretation of spherical particle relaxation time $\tau_{p, sph}$ and non-spherical particle relaxation time, $\tau_{p, nonsph}$.

particle speed up velocity curves, with the number of Subcycles J being the parameter. The results are compared to the correct, analytical solution of Equ.10.

At decreasing numbers of Subcycles, e.g. increasing particle time steps, the speed up curves show increasing deviation from the analytical solution (Figure 2, J = 40, J = 20). If a certain particle time step limit is exceeded, the particle starts experiencing unsteady acceleration (Figure 2, J = 10), and for even higher time steps the numerical solution collapses altogether.

A similar behaviour of the results can be observed if the number of Subcycles is held constant, but the particle diameter, is in turn decreased, or the dynamic fluid viscosity is increased. When drag forces on non–spherical particles are considered, an additional parameter to be taken into account is the local, relative fluid–particle velocity u_{rel}. Here an increase of relative velocity has analogous effect to a decrease of Subcycles.

3. PARTICLE RELAXATION TIME AND STUDY OF NON-SPHERICAL SPEED UP BEHAVIOUR

This chapter will investigate the particle relaxation time τ_p more closely. The well known definition of the particle relaxation for spherical particles will be compared to an expression for the non-spherical particle relaxation time. Moreover the dependence of $\tau_{p,nonsph}$ on local fluid conditions and on the degree of non–sphericity will be investigated. Therefore a new quantification method to describe sphericity will be introduced.

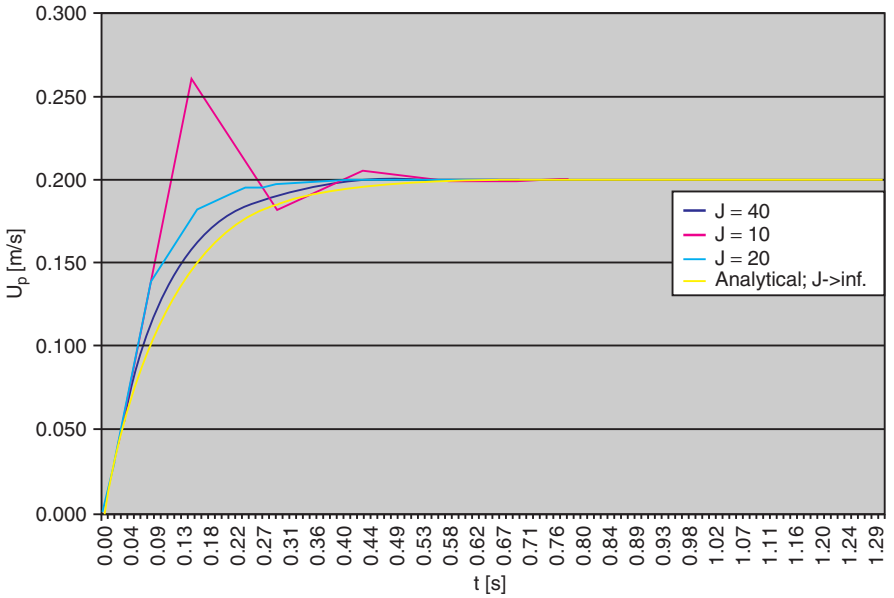

Figure 2 Plot of particle speed up curves for exemplary fluid time step $\Delta t_f = 1.333$s, particle dimension $D_{sph} = 0.01$m, dynamic fluid viscosity $\mu_f = 0.1$Pas, particle density $\rho_p = 2000$ kg/m^3, and uniform flow velocity $u_f = 0.2$m/s. Three numerical speed up curves for static Subcycles J = 40 (blue), J = 20 (turquoise) and J = 10 (purple) are compared to the analytical solution (yellow).

3.1. SPHERICAL PARTICLE RELAXATION TIME

Out of Equ.10 a well known, essential parameter for the particle speed up characteristic can be derived. It defines the time scale for any individual, spherical particle under Stokes drag conditions, is called the spherical particle relaxation time and can be written as:

$$\tau_{p,\,sph} = \frac{D_{sph}^2 \rho_p}{18 \mu_f} \tag{16}$$

The graphical interpretation of the parameter $\tau_{p,sph}$ is given by the intersection point of the speed up curve tangent at t = 0s with the $u = u_f$ line and is depicted in Figure1.

It is worth noting that, by using Stokes' law, $\tau_{p,sph}$ depends only on material properties, regardless of local flow conditions.

By inserting Equ.16 into Equ.10, it can be rewritten as:

$$u_p = u_f - u_{rel,0} \cdot e^{-\frac{t}{\tau_{p,sph}}} \tag{17}$$

3.2. NON-SPHERICAL PARTICLE RELAXATION TIME AND SPEED UP BEHAVIOUR

As previously discussed, Equ.11 yields an expression for a non–spherical particle speed up curve, implicitly containing u_p (within u_{rel}). Equ.11 does not necessarily have to be evaluated numerically for $u_p = f(t)$, to obtain essential parameters of the speed up curve.

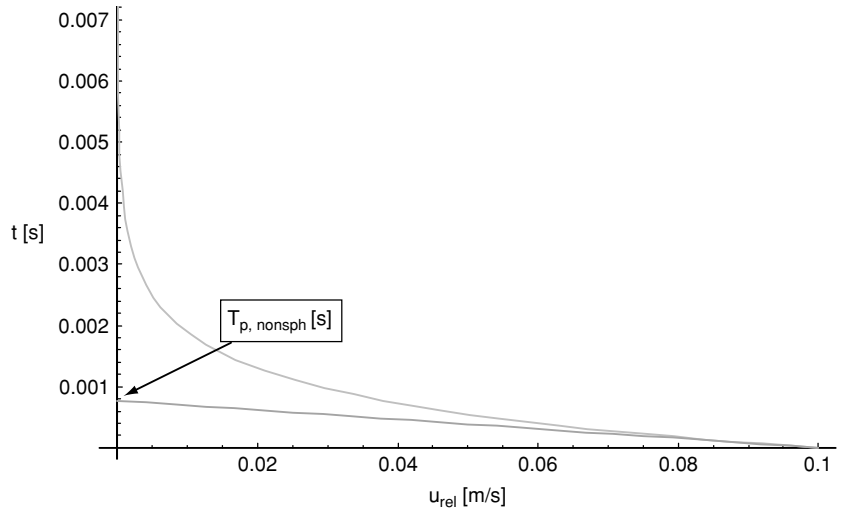

Figure 3 Exemplary plot of non-spherical particle speed up, for D_{sph} = 0.001m, u_f = 0.1m/s, μ_f = 0.1Pas with tangent at t=0s and non–spherical particle relaxation time $\tau_{p,nonsph} = 8*10^{-4}$ s.

Figure 3 shows an exemplary plot of Equ.11 and reveals that the characteristic non–spherical particle relaxation time can be extracted from this implicit expression for u_p as well.

Analogous to the spherical speed up case, the parameter $\tau_{p,nonsph}$ is given by the intersection point of the speed up curve tangent at t = 0 s with the u_{rel} = 0 m/s line. Therefore $\tau_{p,nonsph}$ is defined by:

$$\tau_{p,\,nonsph} = -u_{rel,\,0} \cdot \frac{dt(u_{rel})}{du_{rel}}(u_{rel} = u_{rel,0}) \tag{18}$$

Uniting Equ.18 with the expression for $t(u_{rel})$ out of Equ.11 and with the definitions of C_0, C_1, C_2 and C_3, found in Equ.12 through Equ.15, the non-spherical particle relaxation time for Hölzer/Sommerfeld drag implementation reads:

$$\tau_{p,\,nonsph} = -\frac{C_0}{C_1 + C_2\sqrt{u_{rel}} + C_3 u_{rel}} \tag{19}$$

The non–spherical particle relaxation time, based on Equ.8, depends not only on material properties and particle dimension, but also on the local, relative fluid–particle velocity. As a consequence $\tau_{p,\,nonsph}$ depends on the local particle Reynolds number while $\tau_{p,\,sph}$ does not.

Even an actual particle sphericity of $\Phi = 1$ does not eliminate the velocity dependence in Equ.19. The plot in Figure 4, which holds true for any set of particle properties, shows that, the larger the particle Reynolds number becomes, the worse the accordance of the two τ_p implementations for two identical, spherical particles will be. This reflects the fact that the Stokes version for spherical particle drag is only valid in the *zero* Reynolds limit.

Further evaluation of Equ.19 helps to get an idea of the relationship between particle shape and particle relaxation time. Figure 5 contains a plot of τ_p against Re for particles of varying

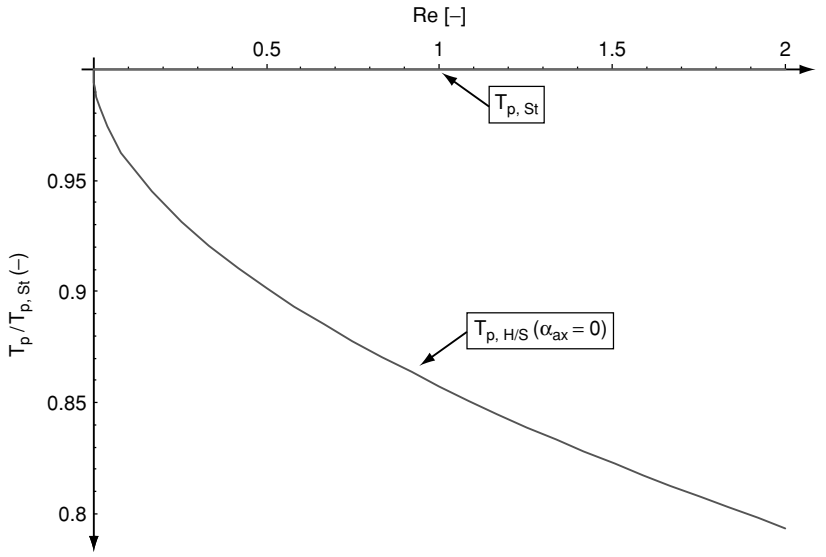

Figure 4 Ratio of spherical particle relaxation time according to Hölzer/Sommerfeld drag $\tau_{p,H/S}$ and spherical particle relaxation time according to Stokes' drag implementation $\tau_{p,St}$ plotted against particle Reynolds number. The higher the Reynolds number, the smaller $\tau_{p,H/S}$ compared to $\tau_{p,St}$. The Stokes' approach loses its validity.

sphericity, but constant D_{sph}. Furthermore Figure 5 demonstrates the basic difference between velocity dependence of "*Stokes' drag spheres"* and *"Hölzer/Sommerfeld ellipsoids"*. In addition to that, the plots in Figure 5 qualitatively show that, the further the particle shape is from being a sphere, the smaller τ_p becomes.

The sphericity can not fully describe the measure of similarity to spherical shape, - crosswise- and lengthwise sphericity are needed as well. Therefore an alternative parameter to measure similarity to a sphere is introduced here. It is the ratio between the standard deviation of the half axis a, b and c around D_{sph}. This parameter shall be denoted as α_{ax} and is defined as:

$$\alpha_{ax} = \frac{\sqrt{\left(2a - D_{sph}\right)^2 + \left(2b - D_{sph}\right)^2 + \left(2c - D_{sph}\right)^2}}{3D_{sph}} \tag{20}$$

Higher values of α_{ax} signify higher deviation from spherical shape and clearly lead to smaller $\tau_{p,nonsph}$ values, which decrease further for higher particle Reynolds numbers. The plot in Figure 5 strongly makes the case for the consideration of particle shape effects in particle calculations. It shows that for values of $\alpha_{ax} \geq 1$, the non–spherical particle relaxation time becomes less than 1/5th of the relaxation time of a volume equivalent sphere.

Figure 6 is a plot of $\tau_{p,nonsph}/\tau_{p,sph}$ against α_{ax}. With the particle Reynolds number being used as parameter, this plot is valid, regardless of material properties or particle diameter D_{sph}. The plot shows that increasing deviation from spherical shape leads to a strong reduction of $\tau_{p,nonsph}$ values. The trend starts levelling of for $\alpha_{ax} \geq 1.5$. Higher particle Reynolds numbers lead to a $\tau_{p,nonsph}$ reduction as well. This effect is more pronounced for nearly spherical particles ($\alpha_{ax} \rightarrow 0$) and mostly within the creeping flow regime (Re < 1).

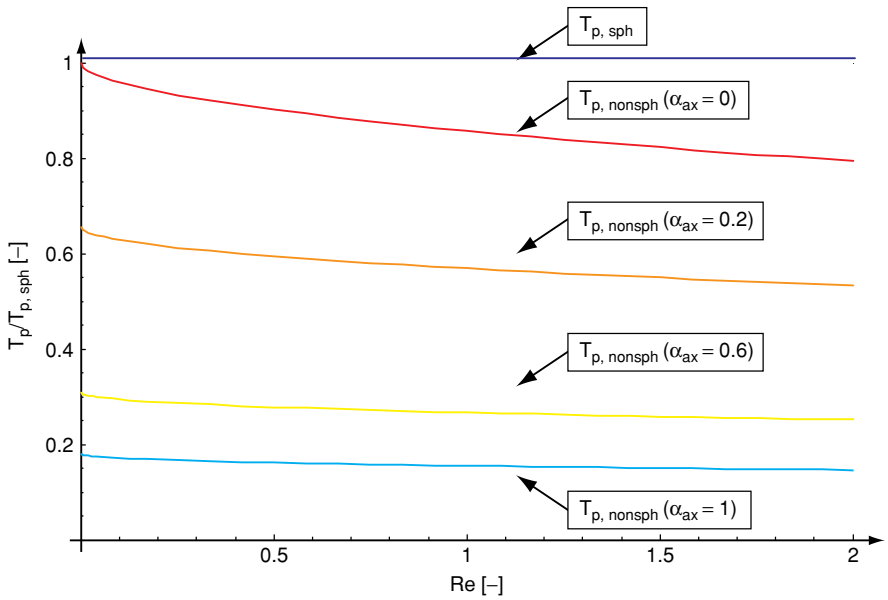

Figure 5 Spherical (blue) and non–spherical (red, orange, yellow, turquoise) particle relaxation time behaviour against particle Reynolds number. Assumtion: a is aligned along fluid stream lines. Increasing α_{ax} (0–1) leads to smaller $\tau_{p,nonsph}$. All values are scaled by $\tau_{p,sph}$ (Re = 0).

The analysis of Figure 6 shows, that the non–spherical particle implementation leads to generally lower relaxation time values than that of the spherical case. Even if the ellipsoid half axis are of equal length (α_{ax} = 0), the non–spherical results deviate from the spherical implementation. Only if the particle Reynolds number reaches the limit Re = 0 and α_{ax} = 0, a match is achieved.

In essence all those insights lead to the conclusion that non–spherical particles have smaller characteristic time scales than volume equivalent spheres. As a consequence they require higher time step resolution. The stronger the non–sphericity, the smaller the time step will have to be to achieve numerical stability.

If maximum efficiency is desired, non–spherical time steps can be increased as a particle accelerates, and relative velocities as well as particle Reynolds numbers decline. However if, on the other hand, the chosen time step criterion is adjusted to the situation of highest possible particle Reynolds numbers, e.g. to the instant of particle injection, it will surely hold for the entire calculation.

3.3. GENERALIZED PARTICLE RELAXATION TIME

The expressions for spherical (Equ.16) and non–spherical (Equ.19) particle relaxation times are given in chapter 3.1 and 3.2 respectively and can easily be extended to a generalized version. It holds for arbitrarily shaped particles and can be written as (Lain, Bröder, Sommerfeld, 1999, [7]):

$$\tau_p = 2\frac{m_p \cdot D_{sph}}{A_f \cdot \mu_f \cdot \mathrm{Re} \cdot cd(\mathrm{Re})} \tag{21}$$

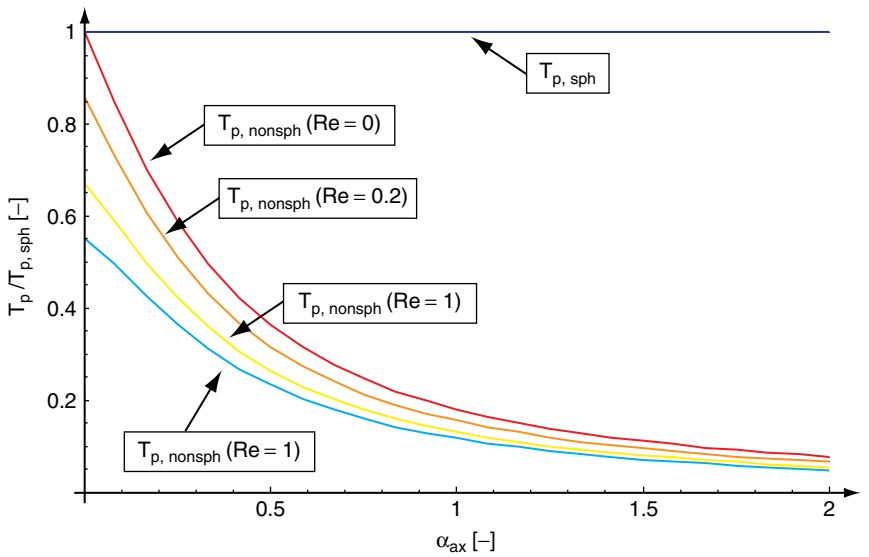

Figure 6 Spherical (blue) and non–spherical (red, orange, yellow, turquoise) particle relaxation time behaviour against relative half axe deviation around D_{sph}. Increasing Re (0–10) and increasing α_{ax} lead to smaller $\tau_{p,nonsph}$. All values are scaled by $\tau_{p,sph}(Re = 0)$.

4. ADAPTIVE TIME STEPPING

After pin-pointing the problem, formulating expressions for particle relaxation times and after examining spherical- as well as non-spherical speed up behaviour, a scheme of Adaptive Time Stepping can be sought. First the multi parameter character of the problem has to be reduced.

4.1. ONE PARAMETER TO DEFINE NUMERICAL STABILITY

By inserting the generalized particle relaxation time τ_p (Equ.21) into the PME (Equ.3) and by consequential, temporal discretization and substitution for $u_{rel} = u_f - u_p$ one obtains:

$$\frac{\Delta t_p}{\tau_p} = -\frac{\Delta u_{rel}}{u_{rel,0}} = \frac{u_{p,t} - u_{p,0}}{u_f - u_{p,0}} \tag{22}$$

Here Δt_p, is the numerical particle sub time step and $u_{p,t}$ is the particle velocity after Δt_p. With Equ.22 a simple formula is given, which relates the ratio of the chosen particle time step and particle relaxation time to the ratio of relative particle–fluid velocity change, Δu_{rel} and relative particle–fluid velocity, $u_{rel,0}$ before Δt_p.

It is quite clear that if the ratio on the right hand side of Equ.22 gets larger than 1, the particle at its new velocity will in any case travel faster than the surrounding flow field. A result like this is not only wrong but will cause the particle to accelerate in the opposite direction in the following time step. As will be shown, a $\Delta t/\tau_p$ ratio of ≥2 will collapse the particle calculation as a whole. The numerical stability of the calculation can only be guaranteed by substantially reducing the $\Delta t/\tau_p$ ratio. It turns out that the terms in Equ.22 are the single most important quantities to measure the extent of numerical (in-)stability of the calculation.

Equ.22 takes the subject away from being a multi parameter problem, which depends on particle dimension, fluid viscosity, fluid velocity and particle density, towards being a single parameter issue, which depends only on the ratio of particle sub time step and particle relaxation time $\Delta t_p/\tau_p$.

The first obvious conclusion is to start scaling the time axis by τ_p and to start expressing the degree of numerical stability by $\Delta t_p/\tau_p$.

4.2. DESCRIBING THE INSTABILITIES

To get a hold of the encountered instabilities, it is first necessary to thoroughly understand and describe them. The key to do that is to consider the iterational effects of the Euler scheme on velocity evolution. Using i as index for the specific iteration at runtime $t = \Delta t_p * i$, Equ.22 can be rewritten to:

$$u_i = u_{i-1} + \frac{u_{rel,0}}{\tau_p}\Delta t_p \tag{23}$$

With particle velocity at iteration $i = 0$ being $u_0 = 0.0$ m/s and with the relative fluid–particle velocity at that time consequentially being $u_{rel,0} = u_f$, the implicit statement of Equ.23 can be transferred into the following explicit expression for u_i:

$$u_i = u_f\left[\left(-1\right)^{i+1}\cdot\left(\frac{\Delta t_p}{\tau_p}-1\right)^{i}+1\right] \tag{24}$$

The evaluation of Equ.24 for various ratios of $\Delta t_p/\tau_p$ is depicted in Figure 7. Obtained results immediately show that Equ.24 accurately explains the encountered instabilities which are partly shown in Figure 2.

By taking a look at Equ.24, the initial assumption (see chapter 4.1), that $\Delta t_p/\tau_p$ is *the* decisive numerical parameter can be confirmed. The following facts can be stated:

1. For $\Delta t_p/\tau_p \leq 1$ and for all $i \in Z$:

$$\lim_{i\to\infty}\left(\frac{\Delta t_p}{\tau_p}-1\right)^{i} = 0 \tag{25}$$

$$\lim_{i\to\infty} u_i = u_f \tag{26}$$

$$\left(-1\right)^{i+1}\cdot\left(\frac{\Delta t_p}{\tau_p}-1\right)^{i} \leq 0 \quad \rightarrow \quad u_i \leq u_f \tag{27}$$

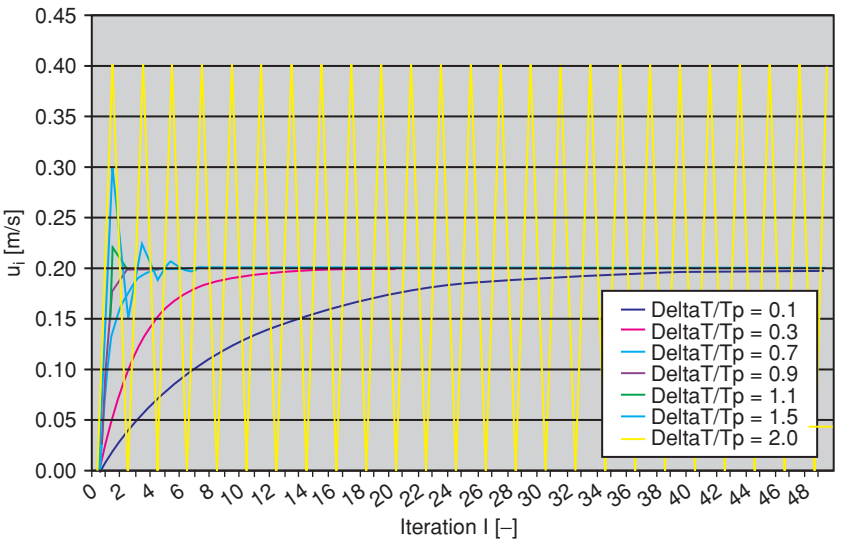

Figure 7 Evaluation of Equ.24 for varying $\Delta t_p/\tau_p$, with u_f = 0.2 m/s. For $\Delta t_p/\tau_p \geq 1$ particle velocity evolution starts showing unsteady behaviour. For $\Delta t_p/\tau_p \geq 2$ the particle calculation collapses. The results accurately match the instability behaviour encountered in the OpenFOAM® solver (Figure 2).

The calculation will remain stable and the particle velocity will steadily converge to u_f. Overall numerical error will increase as $\Delta t_p/\tau_p$ increases.

2. For $1 < \Delta t_p/\tau_p < 2$ and for all $i \in Z$:

$$\lim_{i\to\infty}\left(\frac{\Delta t_p}{\tau_p}-1\right)^i = 0 \tag{28}$$

$$\lim_{i\to\infty} u_i = u_f \tag{29}$$

For all $i \in Z_{even}$:

$$\left(-1\right)^{i+1}\cdot\left(\frac{\Delta t_p}{\tau_p}-1\right)^i > 0 \quad \rightarrow \quad u_i > u_f \tag{30}$$

For all $i \in Z_{uneven}$:

$$\left(-1\right)^{i+1}\cdot\left(\frac{\Delta t_p}{\tau_p}-1\right)^i < 0 \quad \rightarrow \quad u_i < u_f \tag{31}$$

In the $1<\Delta t_p/t_p<2$ regime the particle velocity will eventually converge to $u_{f,}$ just as before, but it will show completely unsteady velocity jumps, oscillating around u_f.

3. For $\Delta t_p/t_p = 2$ and for all $i \in Z$ the particle velocity oscillates unsteadily between $u_i = 0$ and u_f until the geometry boundaries are reached.
4. For $\Delta t_p/t_p > 2$ and for all $i \in Z$:

$$\lim_{i\to\infty}\left(\frac{\Delta t_p}{\tau_p}-1\right)^i = \infty \tag{32}$$

$$\lim_{i\to\infty} u_i = \infty \tag{33}$$

If $\Delta t_p/\tau_p > 2$ the particle velocity will explode and the calculation will collapse. The consequence of this analysis is simple: $\Delta t_p/\tau_p$ must stay well below 1.0 to ensure steady evolution of particle velocity. What remains to be done is to quantify the extent of numerical error within the "regime of steady velocity evolution".

4.3. QUANTIFICATION OF NUMERICAL ERROR

Numerical error is best quantified by considering its effects. Here the resulting speed up curve for any specific $\Delta t_p/\tau_p$ shall be compared to the correct, analytical solution. An explicit, analytical solution is only known for spherical particles, accelerating under Stokes' drag conditions (see Equ.10). For non–spherical particles, the $\Delta t_p/\tau_p$ speed up curve shall be compared to a numerically calculated reference curve, of small, yet basically variable $\Delta t_{p,0}/\tau_p$. As quantitative measure of the overall amount of deviation between numerical and reference results, the medium standard deviation σ shall be chosen. The medium standard deviation is calculated according to Equ.34.

$$\sigma(\Delta t_p/\tau_p) = \sqrt{\frac{\sum_{i=1}^{i_{\max}}[u_{n,i}(\Delta t_p/\tau_p) - u_{a,i}]^2}{i_{\max}}} \tag{34}$$

Here the index *i* indicates the individual, numerical time step, the index *n* indicates a result from the numerical solution for $\Delta t_p/\tau_p$ and index *a*, indicates a result from the reference (analytical) solution. Let the parameter M denote the last compared velocity point at runtime t_{end}, so that:

$$M = \frac{t_{end}}{\tau_p} \tag{35}$$

Then the total number of compared, discrete time steps i_{max} is:

$$i_{\max} = \left\lfloor \frac{M \cdot \tau_p}{\Delta t_p} \right\rfloor \in \mathrm{Z} \tag{36}$$

The exemplary plot of two compared speed up curves in Figure 8 illustrates the numerical error quantification scheme.

4.3.1. Quantification of spherical, numerical error

By using Equ.10 and by representing the particle runtime as $t = \Delta t_p * i$, the analytical solution for iterational particle velocity for spherical particles becomes:

$$u_i = u_f \left(1 - e^{-\frac{\Delta t_p i}{\tau_{p,sph}}} \right). \tag{37}$$

Therefore, the resulting $\sigma(\Delta t_p/\tau_p)$ value for spherical particles can be calculated in accordance with Equ.34 which yields:

$$\sigma_{n-a}\left(\Delta t_p/\tau_p \right) = u_f \sqrt{\frac{1}{i_{\max}} \sum_{i=1}^{i_{\max}} \left[\left(-1\right)^{i+1} \left(\frac{\Delta t_p}{\tau_p} - 1 \right)^i + e^{-\frac{\Delta t_p \cdot i}{\tau_p}} \right]^2} \tag{38}$$

The index *n–a* represents the comparison between the numerical and the analytical solution. To get an idea of the relative deviation, compared to the uniform fluid velocity u_f, the relative medium standard deviation can be written as:

$$\sigma_{rel,n-a}(\Delta t_p/\tau_p) = \frac{\sigma_{n-a}(\Delta t_p/\tau_p)}{u_f} = \sqrt{\frac{1}{i_{\max}} \sum_{i=1}^{i_{\max}} \left[\left(-1\right)^{i+1} \left(\frac{\Delta t_p}{\tau_p} - 1 \right)^i + e^{-\frac{\Delta t_p \cdot i}{\tau_p}} \right]^2} \tag{39}$$

4.3.2. Quantification of non–spherical, numerical error

For non–spherical particles the reference curve shall be created by selecting another speed up curve, based on Equ.24. Therefore a very small $\Delta t_p/\tau_p$ ratio, that serves as the reference value $\Delta t_{p,0}/\tau_p$ has to be chosen. Hence, the resulting $\sigma_{rel}(\Delta t_p/\tau_p)$ value for non-spherical particles is calculated like this:

$$\sigma_{rel,n-n}\left(\frac{\Delta t_p}{\tau_p}, \frac{\Delta t_{p,0}}{\tau_p} \right) = u_f \sqrt{\frac{1}{i_{\max}} \sum_{i=1}^{i_{\max}} \left[\left(-1\right)^{(n-1)\cdot i+1} \left(\frac{\Delta t_{p,0}}{\tau_p} - 1 \right)^{ni} + \left(\frac{\Delta t_p}{\tau_p} - 1 \right)^i \right]^2} \tag{40}$$

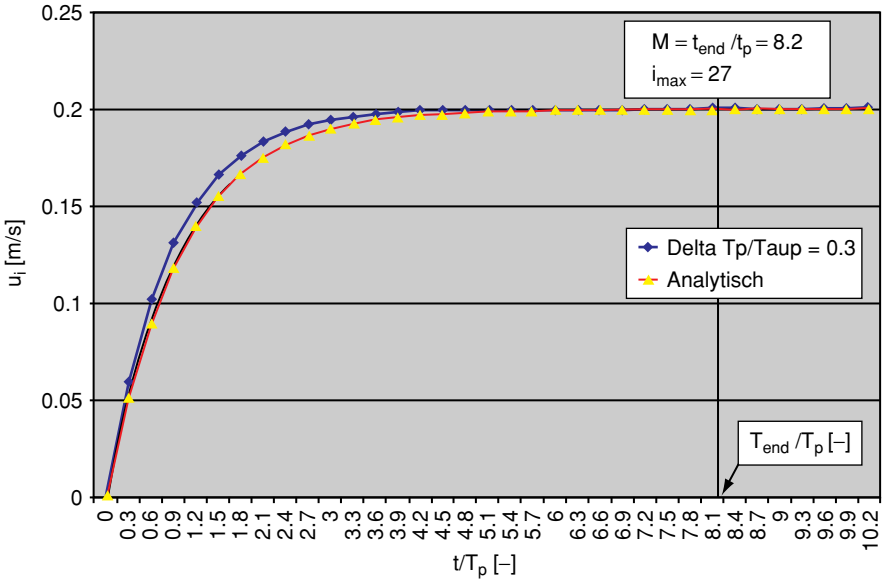

Figure 8 Comparison of analytical (red) and numerical (blue) speed up curve with $\Delta t_p/\tau_p$ = 0.3 and u_f = 0.2m/s. The points of numerical evaluation are shown according to the chosen particle sub time step. To calculate σ, velocity points from t/τ_p = 0.3 to M = t_{end}/τ_p = 8.2 are chosen. In this case the number of compared velocity points is i_{max} = 27.

Here the index n-n represents the comparison between the inspected numerical speed up curve and the numerical reference solution. The new variable n stands for:

$$n = \frac{\Delta t_p}{\Delta t_{p,0}} \in Z \tag{41}$$

The variable n is not to be mixed up with the n used in the indices n-n and n-a.

Of course the reference-value-based, $\sigma_{rel}(\Delta t_p/\tau_p)$ calculation, shown in Equ.40, can also be applied for spherical particles, where an explicit, analytical reference solution is available. In that case the $\sigma_{n\text{-}n}$ value converges to $\sigma_{n\text{-}a}$ as the reference value $\Delta t_{p,0}/\tau_p$ converges to zero:

$$\lim_{\frac{\Delta t_{p,0}}{\tau_p}\to 0} \sigma_{n-n}\left(\frac{\Delta t_p}{\tau_p}, \frac{\Delta t_{p,0}}{\tau_p}\right) = \sigma_{n-a}\left(\frac{\Delta t_p}{\tau_p}\right) \tag{42}$$

.

4.3.3. Evaluation of quantified, numerical error

Based on the quantification procedure described above and in particular based on Equ.39 and Equ.40, extensive parameter studies have been carried out. OpenFOAM® - CFD test runs, featuring spherical and non-spherical particles have been conducted. The particles are set to speed up in a *large* flow channel with *zero* wall friction and thus uniform flow conditions.

Hereby the parameter $\Delta t_p/\tau_p$ was varied, speed up curves were monitored and the $\sigma_{rel}(\Delta t_p/\tau_p)$ values were written out. In parallel, equivalent evaluations, directly based on Equ.39 and Equ.40 were conducted. The results for spherical particles are shown in Figure 9, where the two $\sigma_{rel}(\Delta t_p/\tau_p)$ curves are plotted against $\Delta t_p/\tau_p$. Especially for $\sigma_{rel} \leq 0.2$ the two curves match almost exactly.

The very same figure can be produced for spherical and non–spherical particles, even though the non–spherical CFD calculation uses Hölzer/Sommerfeld drag instead of Stokes' drag, and the non–spherical, analytical curve stems from Equ.40 instead of Equ.39.

A variation of the parameters: fluid velocity, dynamic fluid viscosity, volume equivalent, spherical particle diameter and particle density, confirms the derivations of chapter 4.3. The $\sigma_{rel}(\Delta t_p/\tau_p)$ results show absolutely no dependence on those factors and thus can be considered as universally suitable in terms of particle properties as well as fluid properties and conditions.

Considering Equ.39 and Equ.40, only three further sources of possible influence on the final result remain: the reference parameter $\Delta t_{p,0}/\tau_p$ (relevant for non–spherical particles), the parameter M that affects i_{max} over Equ.36 and the chosen $\Delta t_p/\tau_p$ range. For a discussion of those sources of influence see chapter 4.4.1 to 4.4.3.

The $\sigma_{rel}(\Delta t_p/\tau_p)$ curve shown in Figure 9 however, enables the user to chose a certain $\Delta t_p/\tau_p$ value and immediately get an estimate of the relative standard deviations of evolving, numerical particle velocities, compared to the correct result.

4.4. SIMPLE, LINEAR CORRELATION FOR DEVIATION

Any serious simulation will use values of $\Delta t_p/\tau_p < 0.8$ so that, according to Figure 9, the relative standard deviation to the correct speed up result, will range well below 0.1 (10% u_f). In that region the exponential character of the $\sigma_{rel}(\Delta t_p/\tau_p)$ curve is not yet developed and a linear correlation with a coefficient of determination, $R^2 > 0.99$ can be found. This means that a very simple, linear rule for $\sigma_{rel} - \Delta t_p/\tau_p$ dependence can be obtained. Since for $\Delta t_p/\tau_p = 0$, also $\sigma_{rel} = 0$, the linear correlation bears only *one* degree of freedom, the slope k_{rel}. Hence for $\sigma_{rel} < 0.07$ (7% u_f) we find:

$$\sigma_{rel} = k_{rel} \frac{\Delta t_p}{\tau_p} \tag{43}$$

Figure 10 can be plotted by evaluating the situation shown in Figure 9 for $\Delta t_p/\tau_p$ values that range from 0 to $\Delta t_{p,end}/T_p = 0.55$. It shows the comparison of results yielded by OpenFOAM® and the evaluation of Equ.39. Hereby an almost exact match can be achieved. In this $\Delta t_p/\tau_p$ range a linear correlation with $R^2 = 0.9935$ can be drawn and the resulting slope value k_{rel} can be found to be:

$$k_{rel} = 0.1118 \tag{44}$$

As a consequence the $\sigma_{rel} - \Delta t_p/T_p$ correlation for $\sigma_{rel} < 0.07$ (7%u_f), M = 8.2 and $\Delta t_p/T_p$ values, ranging from 0.0 to $\Delta t_{p,end}/T_p = 0.55$, can be written as:

$$\sigma_{rel} = 0.1118 \cdot \frac{\Delta t_p}{\tau_p} \tag{45}$$

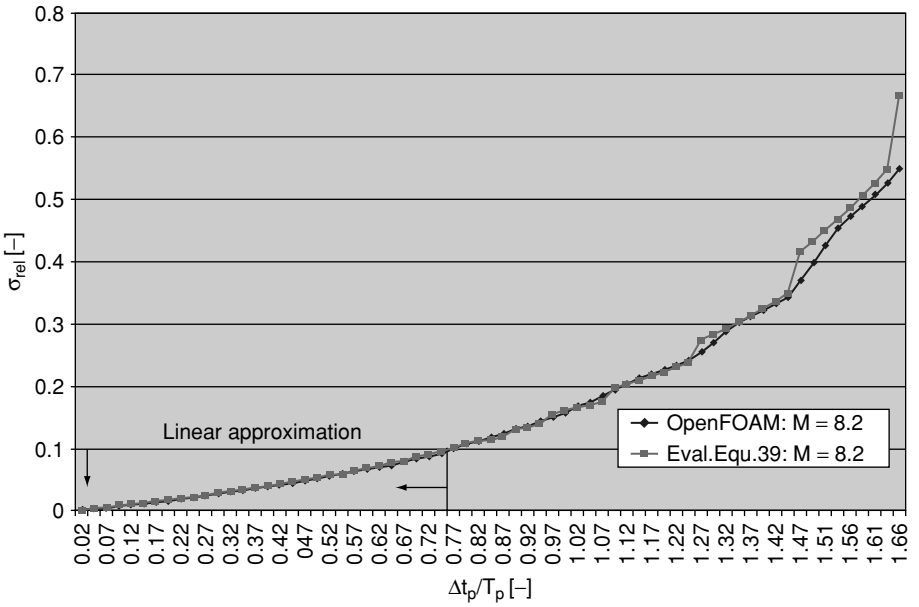

Figure 9 Plot of σ_{rel} against $\Delta t_p/\tau_p$ for a spherical particle of arbitrary size and composition which speeds up in an arbitrary fluid. Each data point is calculated by comparing the corresponding numerical speed up curve to the analytical speed up solution for spherical particles. Comparison of OpenFOAM® implementation (blue) and evaluation of Equ.39 (pink). Chosen M-value is 8.2. The equivalent procedure for an arbitrary, non-spherical particle yields the exact same result.

This holds true for any set of particle properties, for spherical and non–spherical particles and for any set of fluid properties and conditions. By inserting into Equ.45 the user can chose an appropriate $\Delta t_p/\tau_p$ value and immediately estimate its impact on overall numerical deviation to the analytical solution, in relation to the given fluid velocity. On the other hand it is possible to chose a desired, maximum deviation $\sigma_{rel,max}$, and then to immediately estimate the maximum, allowed time step $\Delta t_{p,max}$ for any particle with particle relaxation time τ_p.

To finally decide on the universality of Equ.45, the dependence on parameters like M, the $\Delta t_p/\tau_p$ range and (for non-spherical particles) the reference parameter $\Delta t_{p,0}/\tau_p$ will have to be checked.

4.4.1. Slope dependence on reference value, $\Delta t_{p,0}/t_p$

For non-spherical particles the $\sigma_{rel} - \Delta t_{p,0}/\tau_p$ curve can be calculated by using Equ.40 and by choosing an appropriate reference parameter $\Delta t_{p,0}/\tau_p$. Thus an additional parameter of possible result dependence is introduced. An inspection of dependence magnitude is necessary.

By applying Equ.40 on spherical particles and by letting $\Delta t_{p,0}/\tau_p$ converge to 0.0, the result converges to that of Equ.39. Consequentially it can be concluded that, the lower the value for $\Delta t_{p,0}/\tau_p$ is chosen, the higher the quality of the result will be. To quantify this statement a parameter study for non-spherical particles has been conducted. Therefore the parameter $\Delta t_{p,0}/\tau_p$ has been varied and for each value a full $\sigma_{rel} - \Delta t_p/\tau_p$ correlation, yielding k_{rel} values according to Figure 9, has been established. Using $\Delta t_{p,0}/\tau_p = 0.001$ as starting point, k_{rel} values have been calculated for $\Delta t_{p,0}/\tau_p \leq 0.02$.

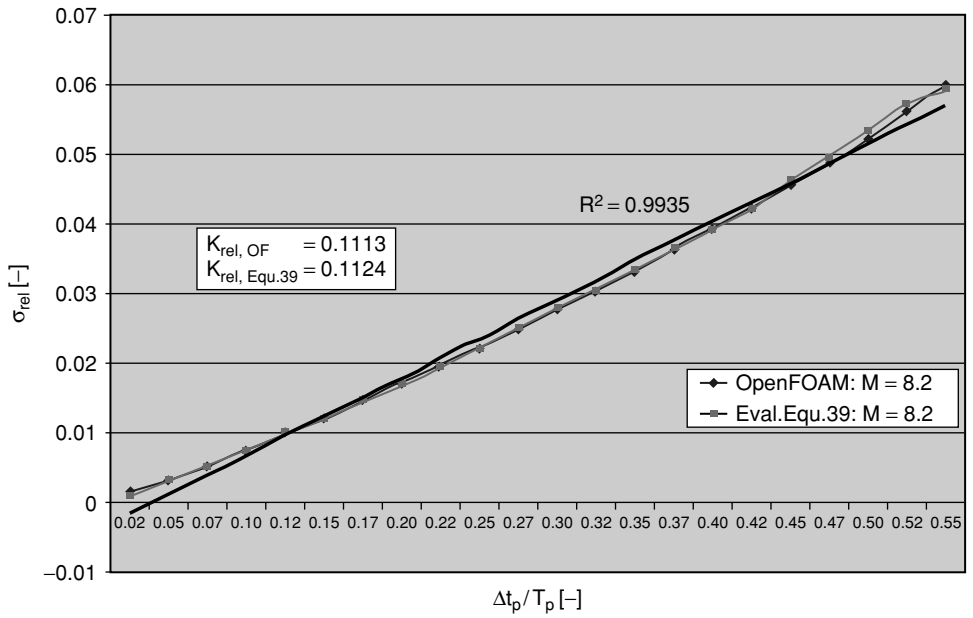

Figure 10 Plot of σ_{rel} against $\Delta t_p/\tau_p$ with $\Delta t_p/\tau_p$ ranging from 0.0 to $\Delta t_{p,end}/\tau_p = 0.55$. Situation is equivalent to Figure 9. Linear correlation with coefficient of determination $R^2 = 0.9935$. Numerical speed up implemented in OpenFOAM® yields a slope of $k_{rel,OF} = 0.1113$ and evaluation of Equ.39 yields slope $k_{rel,Equ.50} = 0.1124$. Results are valid for spherical and non-spherical particles.

The plot in Figure 11 shows that, for $\Delta t_{p,0}/\tau_p < 0.013$, the k_{rel} result deviates by only +/– 5‰ around the starting point result, which means that in this range k_{rel} can be considered to be completely independent of $\Delta t_{p,0}/\tau_p$.

4.4.2. Slope dependence on $M = T_{END}/T_P$

As seen in Figure 8, a variation of the parameter M will almost certainly lead to a change in the calculated, medium deviation between the compared curves. Not to mention the fact that the parameter $i_{max}(M)$ has a profound impact on Equ.39 and Equ.40. Qualitatively it can be stated that:

$$\lim_{M\to 0}\sigma_{rel} = 0 \tag{46}$$

$$\lim_{M\to \infty}\sigma_{rel} = 0 \tag{47}$$

Furthermore it is clear that σ_{rel} will show a maximum somewhere within the range $0 \le M \le \infty$ However it must be noted, that the obvious σ_{rel} – M dependence does not change the numerical situation (e.g. stability) at all. It only brings about a different view point of one and the same numerical speed up curve and its analytical- or reference solution.

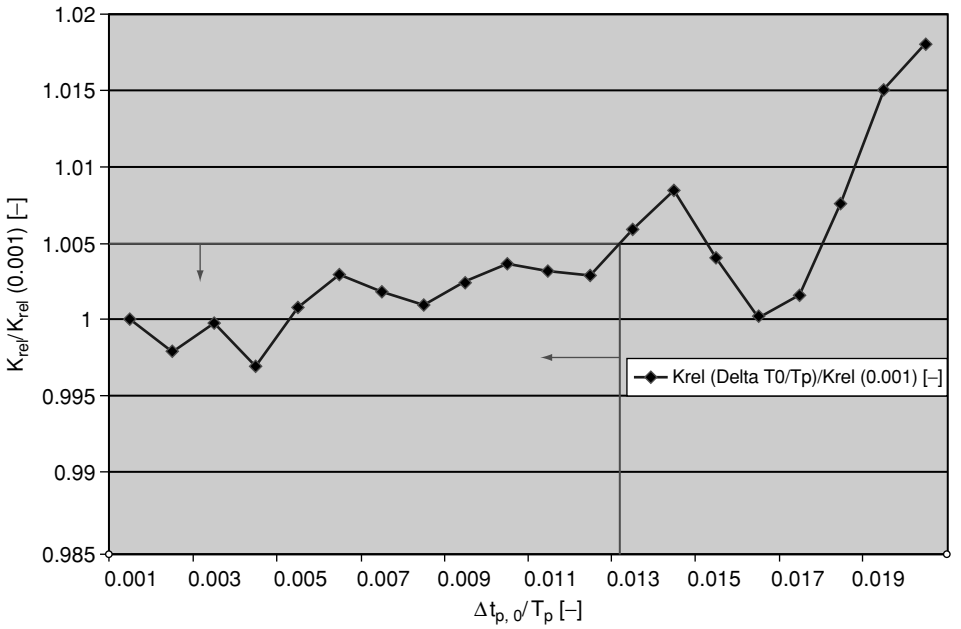

Figure 11 Ratio of $k_{rel}(\Delta t_{p,0}/T_p)/k_{rel}(\Delta t_{p,0}/\tau_p = 0.001)$ plotted against $\Delta t_{p,0}/\tau_p$.

To quantify the $\sigma_{rel} - M$ dependence, and in particular the $k_{rel} - M$ dependence, a parameter study has been conducted. Therefore the parameter M was varied and for each value a full $\sigma_{rel} - \Delta t_p/\tau_p$ correlation, yielding k_{rel} values according to Figure 9, was established. For each calculation of k_{rel} the $\Delta t_p/\tau_p$ value was varied between 0.0 and $\Delta t_{p,end}/\tau_p = 0.15$. Figure 12 shows the resulting plot of k_{rel} against M. As expected: $k_{rel} = 0.0$ for $M = 0$ and also converges to 0.0 for $M \to \infty$. A maximum k_{rel} value $k_{rel,max}$ can be found for $M = 1.60$. It is $k_{rel,max} = 0.170$.

Considering the facts stated above, a reasonable course of action in dealing with the $k_{rel} - M$ dependence is to simply define a constant M value throughout the quantification procedure. Thus a constant, never changing frame of reference is established. A reasonably appropriate point to evaluate the behaviour of the entire speed up curve is the *M-time* $M_{99,9}$, when the accelerating particle has reached 99,9% of the fluid velocity u_f. In that case the ratio between relative fluid–particle velocity and fluid velocity is:

$$\frac{u_f - u_p}{u_f} = \frac{1}{10^p} \tag{48}$$

with, $p = 3$.

Using the analytical speed up solution for spherical particles (Equ.17), $M_{99,9}$ can consequentially be defined as:

$$M_{99,9} = \frac{t_{end}}{\tau_p} = p \cdot \ln 10 \approx 6.91 \tag{49}$$

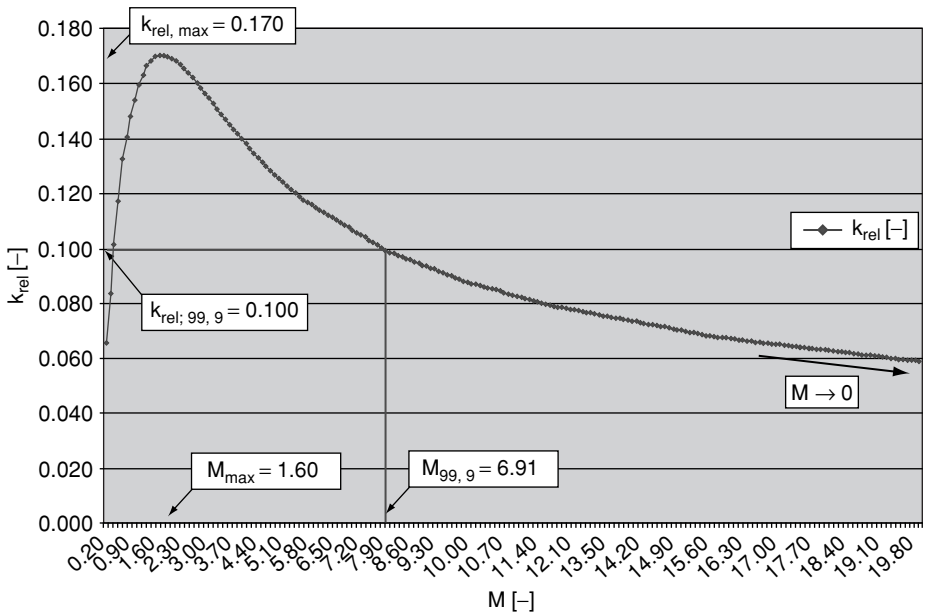

Figure 12 Plot of k_{rel} against M. Maximum k_{rel} value at $M_{max} = 1.60$. Definition of $M_{99,9}$ value and $k_{rel;99,9}$ value.

From Figure 12 the corresponding $k_{rel;99,9}$ value can be derived as:

$$k_{rel,99,9} = 0.100 \tag{50}$$

4.4.3. Slope dependence on $\Delta t_{end}/\tau_P$

A third and final parameter with potential influence on the ultimate k_{rel} result is the $\Delta t_p/\tau_p$ range of possible relative time stepping width, or rather the upper time stepping limit $\Delta t_{p,end}/\tau_p$. While the $\Delta t_p/\tau_p$ values for the linear $\sigma_{rel} - \Delta t_p/\tau_p$ correlation in Figure 9 range from 0.0 to $\Delta t_{p,end}/\tau_p = 0.55$, the k_{rel} – M curve in Figure 12 was calculated for $\Delta t_{p,end}/\tau_p = 0.15$. A qualitative analysis of the $\sigma_{rel} - \Delta t_p/\tau_p$ curve in Figure 9 shows that the higher $\Delta t_{p,end}/\tau_p$, the steeper the "linear" slope k_{rel} will be. For values $\Delta t_{p,end}/\tau_p > 0.8$ a linear correlation is neither appropriate nor necessary.

The basic situation is the same as for the parameters $\Delta t_{p,0}/\tau_p$ and M: a variation does not affect the numerical situation, but only the evaluation of one and the same status. Parameter studies, establishing k_{rel} – M curves (analogous to chapter 4.4.2) for two basic cases of $\Delta t_{p,end}/\tau_p$ have been conducted. The first case, where $\Delta t_{p,end}/\tau_p = 0.15$, holds for $\sigma_{rel} \leq 0.012$ (=1,2% u_f) and the second case, where $\Delta t_{p,end}/\tau_p = 0.04$ holds for $\sigma_{rel} \leq 0.4$ (= 4,0% u_f). Figure 13 shows a direct comparison of the two k_{rel} – M curves.

As expected k_{rel} increases for increasing $\Delta t_{p,end}/\tau_p$, but the basic properties of the curve (convergence and maximum $k_{rel,max}$ at $M_{max} = 1.60$) remain the same. For further applications of the quantification scheme, the $\Delta t_{p,end}/\tau_p = 0.15$ curve will be chosen as reference.

4.5. ADAPTIVE TIME STEPPING OF USER DEFINED ACCURACY

Finally a simple, adaptive time stepping rule, for spherical and non-spherical particles, for any set of fluid- and particle properties and for any given local flow field, can be presented.

For $M_{99,9} = 6.91$ and with $\Delta t_{p,end}/\tau_p = 0.15$ [$\sigma_{rel} < 0.012$ (<1,2%u_f)] the k_{rel} value can be determined out of Figure 13 as:

$$k_{rel;M99,9}^{0.15} = 0.100 \tag{51}$$

So the linear σ_{rel} relation, using Equ.43 reads:

$$\sigma_{rel,M99,9}^{\max 0.012} = 0.100 \cdot \frac{\Delta t_p}{\tau_p} \tag{52}$$

For $M_{99,9} = 6.91$ and with $\Delta t_{p,end}/\tau_p = 0.40$ [$\sigma_{rel} < 0.040$ (< 4%u_f)] the k_{rel} value can be determined out of Figure 13 as:

$$k_{rel;M99,9}^{0.40} = 0.112 \tag{53}$$

So the linear σ_{rel} relation, using Equ.43 reads:

$$\sigma_{rel,M99,9}^{\max 0.04} = 0.112 \cdot \frac{\Delta t_p}{\tau_p} \tag{54}$$

The user can select any desired, medium standard deviation $\sigma_{rel} < 0.040$ (< 4%u_f). Then the appropriate number of particle sub time steps J, that is specifically adapted to the particle as well as the local fluid properties and conditions, can be calculated by use of Equ.2.
For $\sigma_{rel,UD} \leq 1.2\%u_f$:

$$J = \left\lceil 0.100 \cdot \frac{\Delta t_f}{\sigma_{rel,UD} \cdot \tau_p\left(D_{sph}, \rho_p, u_f, \mu_f\right)} \right\rceil \tag{55}$$

For $1.2\%u_f < \sigma_{rel,UD} \leq 4.0\%u_f$:

$$J = \left\lceil 0.112 \cdot \frac{\Delta t_f}{\sigma_{rel,UD} \cdot \tau_p\left(D_{sph}, \rho_p, u_f, \mu_f\right)} \right\rceil \tag{56}$$

5. CONCLUSION

A dirt particle deposition solver, based on the Open Source CFD toolbox OpenFOAM® has been created. The solver is capable of handling spherical and non–spherical particles in the vicinity of realistically reconstructed filter fibre geometries. Due to the specific programming structure of the code, it proved advantageous to use an explicit EULER discretization scheme

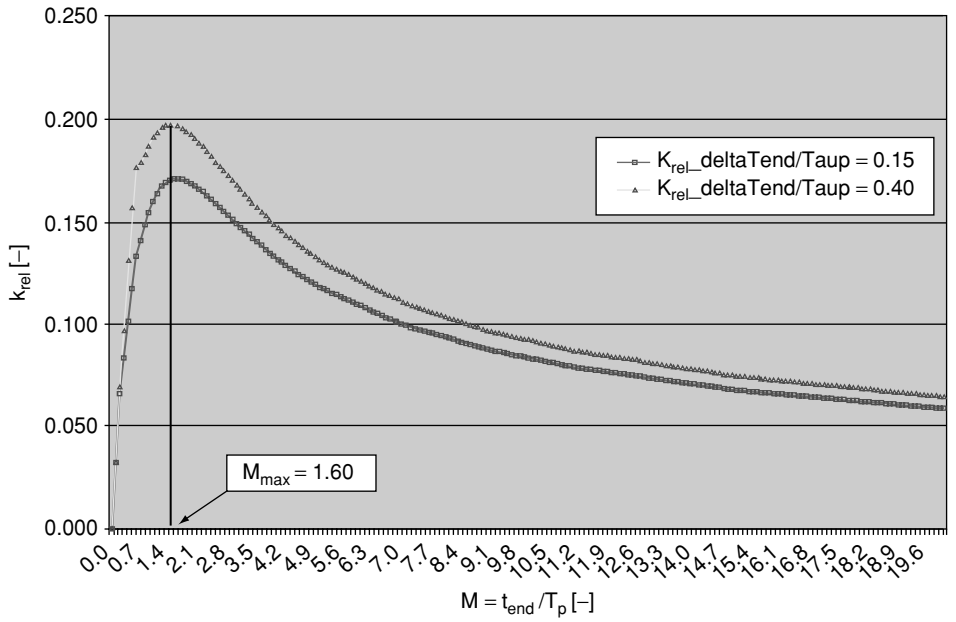

Figure 13 Plot of k_{rel} against M. Chosen parameter is $\Delta t_{p,end}/\tau_p$ = 0.15 (red) and $\Delta t_{p,end}/\tau_p$ = 0.4 (orange). Maximum of both curves lies at M_{max} = 1.60. Difference between curves converges to 0.0 for $M \rightarrow \infty$.

to handle the particle momentum equation. The major drawback of this choice is, that numerical instabilities occur more readily than with other discretization schemes such as the Runga Kutta method. In this work the case of a (non-) spherical particle speeding up in an otherwise uniform, laminar flow field was chosen to describe, study and finally eliminate the encountered numerical instabilities.

The speed up behaviour of spherical and especially non–spherical particles was inspected in detail, and the necessity to consider particle shape deviations from spherical shape was pointed out.

By identifying the parameter $\Delta t_p/\tau_p$ as single most decisive factor for the occurrence of instabilities, the complexity of the problem was dramatically reduced. Particle- and fluid properties as well as fluid conditions can be expressed by τ_p.

In addition to that a descriptive formulation for the instabilities was found, which accurately formulates the problem.

A method to quantify the numerical stability of each speed up run was set up by comparing numerically calculated speed up curves to analytically obtained ones. By producing plots of relative, medium standard velocity deviations against $\Delta t_p/\tau_p$, a simple, linear dependence for low $\Delta t_p/\tau_p$ values was encountered. Thus, by carefully eliminating any possible parameters of influence on the final result, a simple, linear $\sigma_{rel} - \Delta t_p/\tau_p$ relation could be defined, that holds for any set of fluid- and particle properties as well as fluid conditions. This relation enables the user to chose a measure of accuracy (in terms of σ_{rel}) for the simulation run. Out of this choice, the appropriate particle sub time step (the number of particle Subcycles per fluid time step) for each, individual particle, immersed in any local fluid field can be calculated. An adaptive particle time stepping scheme to eliminate instabilities due to explicit Euler implementation can thus be presented.

REFERENCES

[1] M.Mataln, G.Boiger, W.Brandstätter, B.Gschaider, (2008). Simulation of Particle Filtration Processes in Deformable Media, Part 1: Fluid-Structure Interaction, ICE Stroemungsforschung GmbH., Montanuniversitaet Leoben. *Int.Journal of Multiphysics, Vol.2,(No.2), July 2008 , pp. 179–189(11)*;

[2] G.Boiger, M.Mataln, W.Brandstätter, B.Gschaider, (2008). Simulation of Particle Filtration Processes in Deformable Media, Part 2: Large Particle Modelling, ICE Stroemungsforschung GmbH., Montanuniversitaet Leoben. *Int.Journal of Multiphysics, Vol.2,(No.2), July 2008 , pp. 191–206(16)8;*

[3] M.Mataln, W.Brandstätter, (2004). A Unified Approach to Model Fluid-Structure Interactions. Montanuniversitaet Leoben, Austria. *Society of Petroleum Engineering, seminar notes, 2004.*

[4] W.Brandstätter, (2005). *Flow and Combustion Modelling*. Montanuniversitaet Leoben, Austria. Lecture notes February 2005 – July 2005.

[5] C.Crowe, M.Sommerfeld, Y.Tsuji, (1998). *Multiphase Flows with Droplets and Particles*, Boca Raton, FL: CRC Press 1998; ISBN-10: 0849394694/0–8493–9469–4.

[6] R.P.King. *Introduction to Particle Fluid Flow*, Butterworth-Heinemann; (2002).

[7] S.Lain, D.Bröder, M.Sommerfeld, (1999). Experimental and numerical studies of the hydrodynamics in a bubble column. *Chemical Engineering Science, 54, 4913.*

[8] S.Lain, M.F.Göz, (2000). Instabilities in numerical simulations of dispersed two-phase flow. *Mechanical Research Communication, 27, 475.*

[9] S.Lain, M.F.Göz, (2001). Numerical instabilities in bubble tracking in two-phase flow. *International Journal of Bifurcation and Chaos, 11(4), 1169.*

[10] S.Lain, M.F.Göz, (2004). Study of the numerical instabilities in Lagrangian tracking of bubbles and particles in two-phase flow. *Computers and Chemical Engineering 28 (2004) 2727–2733.*

[11] S.Lain, M.F.Göz, M.Sommerfeld, (2006). Instabilities in LaGrangian Tracking of Bubbles and Particles in Two-Phase Flow numerical. *Wiley InterScience, 52: 469–477.*

[12] A.Haider, O.Levenspiel, (1988). Drag Coefficient and Terminal Velocity of Spherical and Non Spherical Particles. *Powder Technology, 58 (1989), 63–70.*

[13] A.Hölzer, M.Sommerfeld, (2007). New, simple correlation formula for the drag coefficient of Non – Spherical Particles. Martin-Luther-Universität, Halle-Wittenberg, Germany. *Powder Technology, Vol.184(3) (2007), 361–365.*

[14] S.V.Apte, K.Mahesh, T.Lundgren, (2003). A Eulerian-Lagrangian model to simulate two-phase/particulate flows, Center for Turbulence Research, Annual Research Briefs, (2003).

[15] W.J.Kowalski, W.P.Bahnfleth, T.S.Whittam, (1999). Filtration of Airborne Microorganisms: Modelling and Prediction. Pennsylvania State University, 1999. *ASHRAE Transactions* 105(2), 4–17. *http://www.engr.psu.edu/ae/iec/abe/publications.*

[16] C.L.Cox, E.W.Jenkins, P.J.Mucha, (2005). Modelling of Debris Deposition in an Extrusion Filter Medium. Clemenson University, Clemenson, SC. Proceedings of the 21st Annual Meeting of the Polymer Processing Society, Leipzig, Germany, June 19–23, 2005.

[17] W. Bohl, W.Elmendorf, (2005). *Technische Strömungslehre*, Vogel Fachbuch, Kamprath Reihe Aufl.:13.2005. ISBN-10: 3834330299.

[18] http://www.opencfd.co.uk/openfoam/

[19] http://www.cfd-online.com/Wiki/CFD-Wiki:Introduction

[20] G.Boiger, M.Mataln, W.Brandstätter, (2009). Simulation of Particle Filtration Processes in Deformable Media, Part 3.1: Basic concepts and particle-fluid force implementation of a non-spherical dirt particle solver, ICE Stroemungsforschung GmbH., Montanuniversitaet Leoben. *Article in review since Jan 2009. Int.Journal of Multiphysics;*

[21] G.Boiger, M.Mataln, W.Brandstätter, (2009). Simulation of Particle Filtration Processes in Deformable Media, Part 3.2: Interaction modelling and solver verification of a non-spherical dirt particle solver, ICE Stroemungsforschung GmbH., Montanuniversitaet Leoben. *Article in review since Jan 2009. Int.Journal of Multiphysics;*